Numerical Study of the Double Diffusion Natural Convection inside a Closed Cavity with Heat and Pollutant Sources Placed near the Bottom Wall

Juan Serrano-Arellano [1], Juan M. Belman-Flores [2],*, Jesús Xamán [3], Karla M. Aguilar-Castro [4] and Edgar V. Macías-Melo [4]

[1] Instituto Tecnológico Superior de Huichapan, ITESHU-TecNM, Huichapan, Hidalgo 42411, Mexico; jserrano@iteshu.edu.mx

[2] Engineering Division, Campus Irapuato-Salamanca, University of Guanajuato, Salamanca 36885, Mexico

[3] Centro Nacional de Investigación y Desarrollo Tecnológico, CENIDET-TecNM, Cuernavaca 62490, Mexico; jxaman@cenidet.edu.mx

[4] División Académica de Ingeniería y Arquitectura, Universidad Juárez Autónoma de Tabasco, Cunduacán 86690, Mexico; karla.aguilar@ujat.mx (K.M.A.-C.); edgar.macias@ujat.mx (E.V.M.-M.)

* Correspondence: jfbelman@ugto.mx; Tel.: +52-464-647-9940

Abstract: A study was conducted on the double diffusion by natural convection because of the effects of heat and pollutant sources placed at one third of the closed cavity's height. The heat and pollution sources were analyzed separately and simultaneously. The study was considered for the Rayleigh number interval $10^4 \leq Ra \leq 10^{10}$. Three case studies were analyzed: (1) differentially heated closed cavity with only heat sources; (2) differentially heated closed cavity with only pollutant sources; and (3) differentially heated closed cavity with heat and pollutant sources. The governing equations of the system were solved through the finite volume technique. The turbulence solution was done with the k-ε model. The dominant influence of the buoyancy forces was found due to the pollutant diffusion on the flow pattern, and an internal temperature increase was observed with the simple diffusion. The most critical case was obtained through the double diffusive convection with an average temperature value of 32.57 °C. Finally, the Nusselt number increased as the Rayleigh number increased; however, the Sherwood number either increased or decreased when the Rayleigh number increased. The highest mean concentration recorded was 2808 ppm; this was found with the value $Ra = 10^6$.

1. Introduction

The natural convection phenomenon is studied due to its several applications in engineering, for instance enclosed spaces. Its applications go from the field of electronics, for heating up or cooling down closed cavities, to applications in buildings as enclosed places, e.g., when a group of people (users) gather for a specific purpose. This situation occurs at an office, a classroom, an auditorium, and other similar places. Various studies devoted to the natural convection phenomenon produced by buoyancy forces due to a heat gradient are found in the literature. Few studies are found detecting that the convective movement is produced by the double diffusion. For example, Łukaszewicz and Kalita [1] carried out a study with practical applications that have the flow of fluids through the Navier–Stokes equations, showed various sections addressing different techniques for solving problems in the field of fluids.

In the present study, the mass equation is part of the system of governing equations, to include the convective diffusion of the pollutant concentration transported by the mass airflow. The purpose is to the distribution of pollutants inside an enclosure. Reviewing the literature, the following studies found are classified into two groups, the first is focused on closed cavities. For instance, Das and Basak [2] performed a numerical study of a closed cavity; they used the finite element method to obtain the solution. Different locations of the heat source were considered to obtain different configurations. *Nu* number values were obtained and increases in convective flow were observed with the *Ra* number increment. Finally, the authors found the most efficient configuration. Hua-Shu and Gang [3] performed a numerical study of a differentially heated rectangular cavity which contains a heated filament on the inside as a heat source. The finite volume method was used to solve the numerical model. The length of the filament was varied to observe the behavior of the heat flow. The results show that the best location of the heated filament was in the center of the cavity. Hassan et al. [4] conducted a numerical study of a square cavity differentially heated to find the appropriate insulation thickness to avoid heat transfer in spaces for residential or industrial use.

In another study, Kouroudis et al. [5] performed a numerical study of the direct simulation of a square cavity; the technique used was that of finite volume. The value of the number of *Ra* was varied to analyze the structure of the flow. Kefayati [6] performed a numerical study of a porous square cavity containing a non-Newtonian nanofluid; the numerical technique used was Finite Difference Lattice Boltzmann Method (FDLMB). The author carried out a parametric study of different non-dimensional numbers such as *Ra*, Darcy, Prandtl, and others. The author showed the relationship of the increase of the heat and mass transfer with the increase of the *Ra* number. Moreover, Miroshnichenko and Sheremet [7] performed a numerical study in a turbulent flow regime of a square cavity with a heat source inside. The numerical technique used was the finite differences method. The emissivity and conductivity were varied to find the Nu number values. Parmananda et al. [8] performed a numerical study of a cubic cavity to analyze convective and radiative heat transfer. The authors set the study parameters for different configurations to obtain the differences in the *Nu* number value and find the optimal configuration. Kefayati [9] performed a numerical study of the natural convection in a porous cavity filled with Bingham fluids. The square cavity was subject to a temperature gradient. The numerical technique was the lattice Boltzmann method and the parameters varied were *Ra*, *Da*, ε (porosity), and *Bn* numbers. The results indicate that for specific Ra and *Da* numbers the Bingham number increases. A brief description of the works of closed cavities with heat and mass transfer was made; in all of them, it was observed that the mass transfer was not addressed as a concentration of water vapor.

An experimental study of heat and mass transfer in a small closed cavity was presented by Kamotani et al. [10], who imposed the gradients through an electrochemical system to observe the flow structures. Bennacer and Gabin [11,12] numerically analyzed the double diffusion convection of a binary fluid contained in a two-dimensional enclosure. The study was also based on horizontal temperature and concentration gradients. Lee et al. [13] analyzed the natural convection of a saltwater solution and observed two types of flow fields (single-celled and multilayer) depending on the magnitude of the buoyancy ratio. Eyden et al. [14] studied the double diffusion by natural convection in turbulent flow numerically and experimentally, considering a mixture of gases. They defined a condition of transient thermal stratification for the bottom hot wall. The authors concluded on some differences in the vertical velocity profile due to three-dimensional effects. Joubert et al. [15] numerically studied heat and mass transfer by natural convection with turbulent flow in a cavity. The authors studied the influence of various models of turbulence (DNS, LES, and RANS) with discrepancies of less than 25%. They concluded that the DNS and LES models presented a higher thermal stratification.

Fu-Yun et al. [16] performed a numerical model of double diffusion by natural convection for a rectangular cavity, which was filled with a binary fluid in a porous medium. The results show a delay effect of the flow and the diffuse transport of heat and mass when decreasing the Darcy number. Kuznetsov and Sheremet [17] numerically analyzed conjugate heat and mass transfer by natural

convection in a square, closed cavity. In the study, a heat source was attached to the bottom surface as well as a source of contaminants on the right side of the bottom wall. The authors concluded on the influence of the Grashof number on the flow pattern by increasing or decreasing the diffusion process. Nikbakhti and Rahimi [18] studied natural convection double diffusion in a rectangular cavity in laminar flow by fixing sources of heat and contaminants on vertical walls and at certain positions in the cavity. They concluded that the heat and mass transfer increased for the upper and lower configurations that represented the airflow inlet. Chen and Du [19] evaluated the double convection-diffusion of natural turbulence in a rectangular cavity. The authors studied entropy generation by varying the Rayleigh number, buoyancy ratio, and aspect ratio. The entropy generation was not sensitive to $Ra \leq 10^9$. Ibrahim and Lemonnier [20] studied a square cavity with a mixture of N_2 and CO_2, considering the transient double diffuse convection coupling with opposite and assisted flow radiation. The authors concluded that gas radiation influences velocity structure and thermal fields.

Recently, Serrano-Arellano et al. [21] numerically studied the transfer of heat and mass by natural convection in a square cavity with an air–CO_2 mixture. The study was based on temperature and concentration gradients and the transition from laminar to turbulent flow. For high Rayleigh numbers and equilibrium buoyancy forces, the temperature was found to correspond to a comfort zone. Finally, Serrano-Arellano et al. [22] analyzed the effect of point sources of pollutants (CO_2) on heat and mass transfer in a closed cavity. They concluded that point sources located near the lower wall decreased air temperature, while those located near the upper wall decrease concentration levels.

The present study analyzed the phenomenon of double diffusion in a differentially heated closed cavity with a turbulent flow regime. The double diffusion was caused by sources of contaminants located inside the closed cavity. The dimensions of the differentially heated closed cavity were varied, and three case studies were compared: (1) differentially heated closed cavity with only heat sources; (2) differentially heated closed cavity with only pollutant sources; and (3) differentially heated closed cavity with heat and pollutant sources. The authors based on the literature review consider that a configuration such as that presented in the present study has not been reported in either a laminar or turbulent flow regime. The contribution of this research will be for a better understanding of the effect of heat and/or pollutant sources located inside a differentially heated closed cavity. The practical applications of this study are in the field of thermal comfort and air quality in closed rooms modeled as closed cavities.

2. Problem Definition

The physical configuration consisted of a rectangular room modeled as a 2D differentially heated square cavity (T_H = 35 °C and T_C = 15 °C), with four-point heat and pollutant sources located at a height of $H_y/3$, as shown in Figure 1. The pollutant sources were fixed at a constant value of 3000 ppm, whereas the prescribed temperature values at the same location were kept at 35 °C, representing people sitting on chairs and generating heat and CO_2 in classrooms, offices, or training rooms. The horizontal and vertical surfaces of the enclosure were impermeable, and the horizontal surfaces were thermally insulated. The Rayleigh number was varied from 10^4 to 10^{10} to cover a broad range of flow regimes. The thermo-physical properties of the fluid were estimated by using the procedure described by Reid et al. [23] as ρ = 1.1852 kg/m^3, λ = 0.03356 W/m K, μ = 1.9198 × 10^{-5} kg/m s, c_p = 1043.1735 J/kg K, and D_{AB} = 1.6966 × 10^{-5} m^2/s. The dimensionless parameters considered in the present study were calculated as Lewis number of 1.6 (*Le*) and the Rayleigh number of $Ra = g\beta(T_H - T_C)L^3/\nu\alpha$, where L is the length of the convective wall. The coefficients of thermal expansion $\beta = (T_{average})^{-1}$ and volumetric expansion $\beta_C = (C_{average})^{-1}$ were calculated. The study was carried out considering the following assumptions: two-dimensional geometry, steady state, incompressible fluid, Newtonian fluid, no viscous dissipation, and thermal radiation exchange was neglected. All thermophysical properties were assumed to have a constant temperature, except for the density in the buoyancy term (Boussinesq approximation). The energy flux produced by the mass transfer (Dufour effect) and the

mass flux caused by the energy transfer (Soret effect) were not considered. Finally, the fluid properties were evaluated at a reference temperature of $T_0 = (T_H + T_C)/2$.
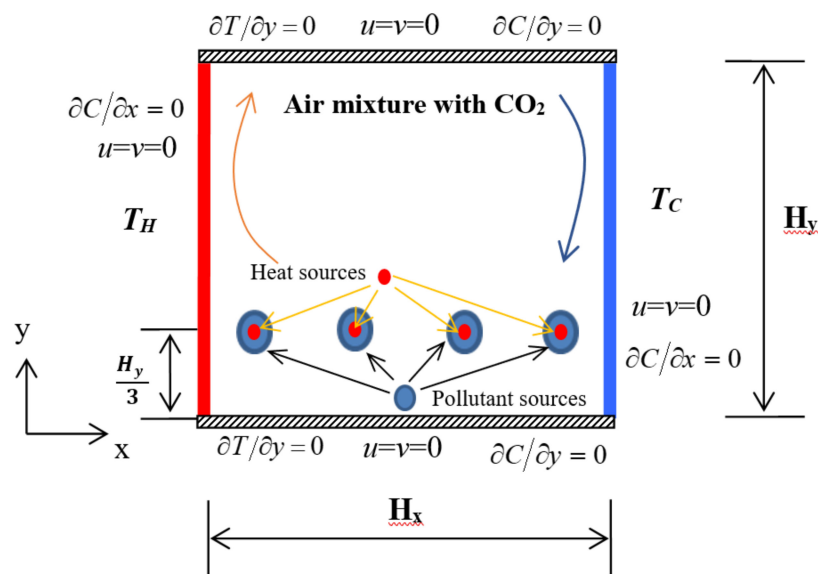

Figure 1. Physical configuration.

Mathematical Model

Considering the above physical assumptions, the governing differential equations of mass, momentum, concentration, and energy in steady state and for turbulent flow can be expressed as follows:

$$\frac{\partial(\rho u_i)}{\partial x_i} = 0 \tag{1}$$

$$\frac{\partial(\rho u_i u_j)}{\partial x_j} = -\frac{\partial P}{\partial x_i} + \frac{\partial}{\partial x_j}\left[\mu\left(\frac{\partial u_i}{\partial x_j} + \frac{\partial u_j}{\partial x_i}\right) - \overline{\rho u_i' u_j'}\right] + \rho g_i \beta(T - T_\infty) + \rho g_i \beta_C(C - C_\infty) \tag{2}$$

$$\frac{\partial(\rho u_j T)}{\partial x_j} = \frac{1}{c_p}\frac{\partial}{\partial x_j}\left(\lambda\frac{\partial T}{\partial x_j} - c_p \overline{\rho u_i' T'}\right) \tag{3}$$

$$\frac{\partial(\rho u_j C)}{\partial x_j} = \frac{\partial}{\partial x_j}\left(\rho D\frac{\partial C}{\partial x_j} - \overline{\rho u_j' C'}\right) \tag{4}$$

The system in Equations (1)–(4) governs the physical phenomenon of heat and mass transfer. Equations (1)–(4) contain the diffusive and convective terms for fluid modeling, and are widely used in numerical studies [24,25]. The two transport equations of the *k-ε* turbulence model used to close the problem are:

$$\frac{\partial(\rho u_i k)}{\partial x_i} = \frac{\partial}{\partial x_i}\left[\left(\mu + \frac{\mu_t}{\sigma_k}\right)\frac{\partial k}{\partial x_i}\right] + P_k + G_k - \rho\varepsilon \tag{5}$$

$$\frac{\partial(\rho u_i \varepsilon)}{\partial x_i} = \frac{\partial}{\partial x_i}\left[\left(\mu + \frac{\mu_t}{\sigma_\varepsilon}\right)\frac{\partial\varepsilon}{\partial x_i}\right] + C_{\varepsilon 1}[P_k + C_{\varepsilon 3}G_k]\frac{\varepsilon}{k} - C_{\varepsilon 2}\frac{\rho\varepsilon^2}{k} \tag{6}$$

Equations (5) and (6) represent the *k-ε* turbulence model, which has given a good approximation in numerical results [26,27] and thus is used in studies of closed or ventilated cavities.

Many authors have suggested various empirical constants for the *k-ε* turbulence model such as $C_{\varepsilon 1} = 1.44$, $C_{\varepsilon 2} = 1.92$, $C_\mu = 0.09$, $\sigma_k = 1.0$, and $\sigma_\varepsilon = 1.3$. In particular, the constant $C_{\varepsilon 3} = tanh|v/u|$ was selected following the HH model proposed by Henkes [28]. The mathematical boundary conditions

were defined as follows: on all solid surfaces, the non-slip condition was valid ($u = v = 0$); on vertical walls, the temperature was kept at a constant value of $T = T_H$ in $x = 0$ and $T = T_C$ in $x = Hx$; a local concentration of CO_2 was kept at a constant value of $C = C_H$ for each source location in *(Hx/5, Hy/3)*, *(2Hx/5, Hy/3)*, *(3Hx/5, Hy/3)*, *(4Hx/5, Hy/3)* and without concentrations on vertical walls; and the horizontal surfaces were considered as impermeable and adiabatic ($\partial T/\partial y = 0$, $\partial C/\partial y = 0$) in $y = 0$ and $y = Hy$). The non-dimensional heat transfer (Nusselt number) is given by:

$$Nu = \frac{\left(-\lambda(\partial T/\partial \eta)_{wall}\right)Hx}{\lambda \Delta T} \tag{7}$$

3. Solution Approach

The numerical procedure to solve the governing Equations (1)–(6) is based on the finite volume method [29]. The generalized equation of transfer is:

$$\frac{\partial}{\partial x_j}\left(\rho u_j \phi\right) = \frac{\partial}{\partial x_j}\left(\Gamma \frac{\partial \phi}{\partial x_j}\right) + S_\phi \tag{8}$$

When integrating a finite control volume, the governing equation becomes an algebraic equation expressed as:

$$a_P \phi_P^{n+1} = \sum_{nb} a_{nb} \phi_{nb}^{n+1} + S_\phi \Delta V + \rho^n \Delta V \phi_P^n \tag{9}$$

where n and nb represent the number of iterations and the coefficient for the adjacent nodes, respectively. The convective terms are formulated by the power law scheme and the diffusive terms are formulated by the central scheme. The coupling between equations was done through the algorithm SIMPLEC, proposed by Van Doormal and Raithby [30]. The method of solution adopted was line by line (LBL) with the alternating direction implicit (ADI) scheme. A low-relaxation factor was applied to improve the convergence of the model. What follows is a general description of the numerical procedure: (1) initial values were proposed (u, v, T, C,...ε); (2) the distributions of speeds and pressure were calculated (u, v, p) through the SIMPLEC algorithm; (3) the range of temperature (T), the range of CO_2 concentrations (C), the range of the kinetic energy of turbulence (k), and the dissipation rate of the kinetic energy of turbulence (ε) were recalculated; and (4) the iteration was done using the convergence criterion until a residual criterion of 1×10^{-8} was achieved.

Verification of the Numerical Code

Various verifications of the developed numerical code were carried out, and a comparison was done with the study by Béghein et al. [31] where the heat and mass transfer were analyzed by natural convection in a laminar flow regime for a closed cavity. The study was performed for a value of the Rayleigh number at 10^4. In Figure 2, the comparison of the values of the Nusselt number and the local Sherwood number on the hot wall is shown. The comparison presented a maximum difference of 2.91% at a height of 0.845.

Another comparison of the numerical code was made with a study of heat transfer by natural convection in turbulent flow regime by Henkes et al. [32]. The study was carried out for the differentially heated cavity for a value of the Rayleigh number of 5×10^{10}. The comparison was made with the average, mean, and maximum Nusselt number, horizontal speed components, and vertical speed components for the mean values. In Table 1, the percentage difference of the values is observed.

One last validation process of the numerical code is a comparison with the experimental Benchmark study in [33] (see Figure 3). A similar verification is presented in [22]. A Rayleigh number of 1.58×10^9 was considered. Velocity (v), temperature (T), turbulent kinetic energy (k), and wall shear stress $\left(\overline{u'v}\right)$ with a HH turbulence model are shown in graphical form in Figure 3.
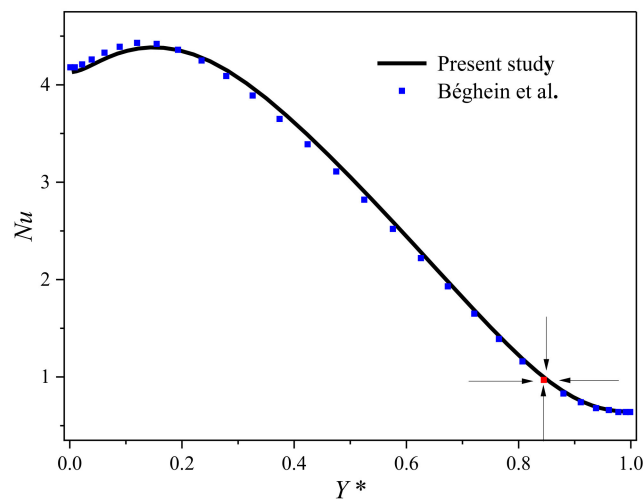
Figure 2. Comparison of the results in this study with the results by Béghein et al. [31].

Table 1. Comparison with the results by Henkes et al. [32].

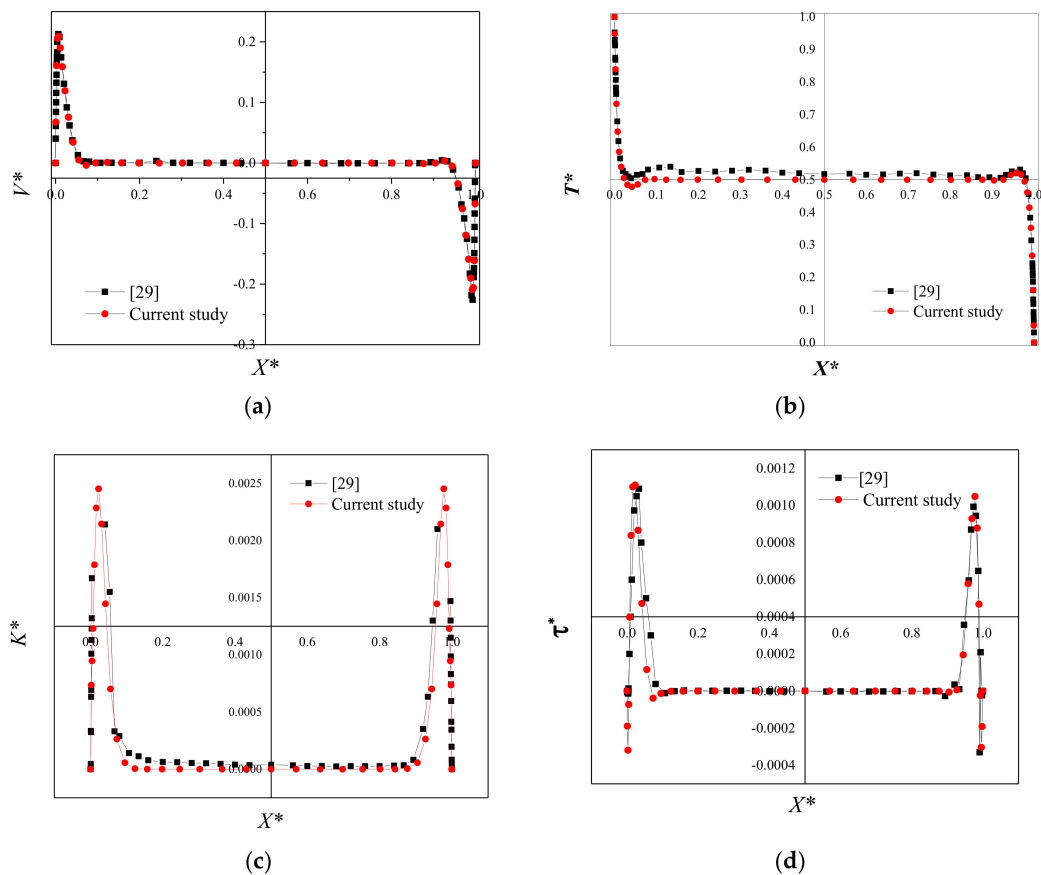| Parameters of Comparison (Reference Interval)	Henkes et al.	Present Study	Difference (%)
$Nu_{average}$ (249−261)	256.0	237.9	7.07
$Nu_{y=Hy/2}$ (256−268)	261.0	262.8	0.68
Nu_{max} (717−750)	730.0	749.7	2.69
$v_{max,\,y=Hy/2}$ (0.167−0.168)	0.167	0.166	0.59
$u_{max,\,x=Hy/2}$ (0.167−0.168)	0.0124	0.0113	8.87

(**a**)

(**b**)

(**c**)

(**d**)

Figure 3. Comparison of non-dimensional variables V^*, T^*, K^*, and τ^* at the center of the cavity.

Once the verification of the numerical code was done, a mesh independence study was carried out, for which the mesh density was increased in the directions of the coordinate axes. The increments were of 10 additional computational nodes to each case, from 71×71 to 91×91. Finally, it was found that, with a mesh of 101×101 computational nodes, there was no significant change in the variables of interest (less than 0.02% in the average Nusselt number) with these values of the computational nodes, thus we proceeded to perform the numerical study.

4. Results and Discussions

Figure 4 shows the effects of the heat sources located inside the cavity in accordance with the *Ra*. It was observed that, with the increase of the *Ra*, the internal sources affected the behavior of the flow pattern because it was distorted, as seen on the current lines. For low values of *Ra*, that is $Ra = 10^4$, it was observed that the behavior was similar to the one presented using the differentially heated cavity in laminar flow regime. However, for a turbulent flow regime, the behavior changed compared with the same conditions of the differentially heated cavity. It was clear that, for high values of *Ra*, that is 10^{10}, the flow pattern was distorted, and different recirculations in various sizes were formed inside the cavity. Furthermore, the different intensities in the flow pattern defined the convection movement inside the cavity. The recirculations were formed due to the pressure exerted by the buoyancy forces (generated by the heat sources) on the flow main mass.

The description of the isotherms in Figure 4b clearly shows how the temperatures tended to homogenization inside the cavity when *Ra* increased. For the values of *Ra* in the interval from 10^4 to 10^6, the behavior was similar to the one presented in the differentially heated cavity. However, as the *Ra* increased, the internal temperatures tended to homogenize between 24 and 27 °C due to the convection movement inside the cavity; the rise in the convective movement was caused by the internal heat sources, which were uniformly placed and helped increase the buoyancy forces.
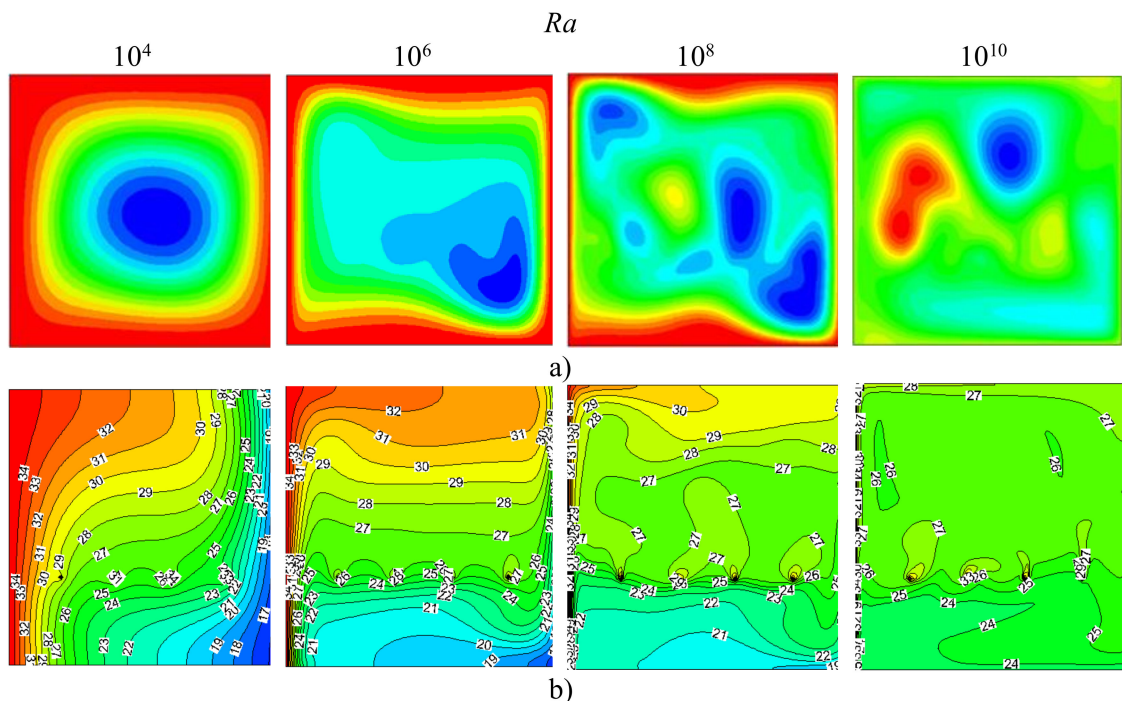

Figure 4. Effect of the heat sources inside the cavity: (**a**) flow patterns; and (**b**) isotherms with internal heat sources.

In Figure 5, the effect of the pollutant sources, located inside the differentially heated cavity, as the *Ra* increased, is observed. It is possible to observe that the flow pattern formed a big recirculation for the low values of the *Ra* number (10^4). Afterwards, when the *Ra* value increased, two recirculations

were formed inside the cavity, which was caused by the impulse of the buoyancy forces generated by the pollutant forces located inside the cavity. This behavior appeared from the value of $Ra = 10^2$ and remained steady as the Ra value increased.
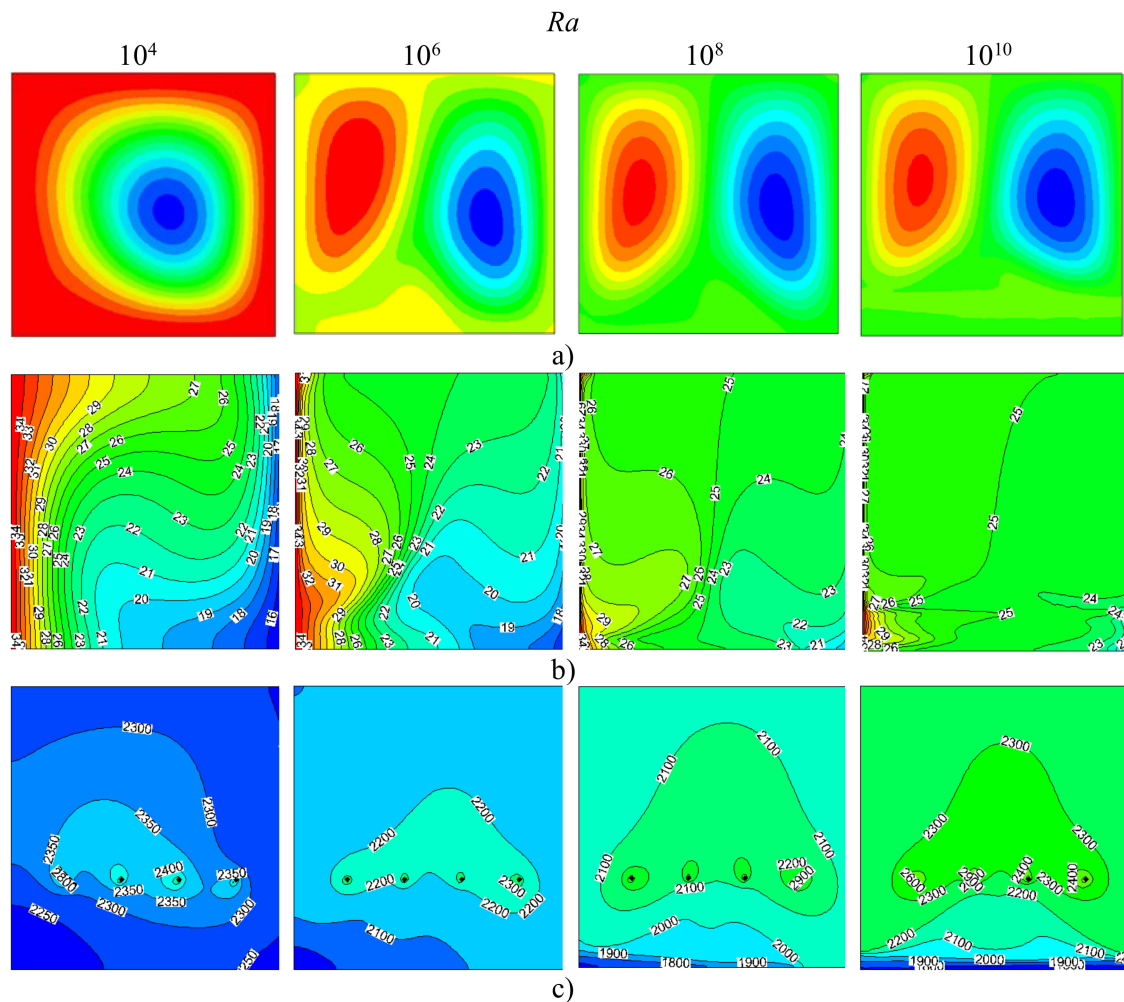

Figure 5. Effect of the pollutant sources inside the cavity: (**a**) flow patterns; (**b**) isotherms without internal heat sources; and (**c**) isoconcentrations with internal concentrations sources.

In Figure 5b shows that the temperatures pattern was distorted by the pollutant sources, which was more notable for the low Ra values ($Ra \leq 10^6$); nevertheless, when the Ra became higher, the isotherms tended to agglutinize inside the cavity, near the hot and cold walls, respectively. It is worth noting, however, that the temperatures values had a tendency to a constant value, which meant that the rise in the flow intensity tended to homogenize the values of the variables inside the cavity.

On the other hand, the pollutant sources shown in Figure 5c displayed that their effect is more evident in small areas around the pollutant sources for low values of Ra ($Ra = 10^4$). The areas surrounding the pollutant sources started to take a bell shape as the Ra increased. When the Ra took the highest value ($Ra = 10^{10}$), it was observed that there was a thin strip showing less pollutant concentration, very close to the bottom wall. In the rest of the cavity, the pollutant concentration homogenized, and a parabola was formed below the pollutant sources. The described behavior is caused by the buoyancy forces that interacted with the recirculatory movement generated by the differentially heated cavity.

Figure 6 shows the effect caused when heat and pollutant sources were simultaneously active inside the closed cavity. It can also be observed that the flow pattern remained virtually the same as

when applying only pollutant sources, meaning that the behavior pattern was defined by the pollutant sources, and thus the heat sources showed no influence. Nonetheless, a change in the behavior of the isotherms was observed (Figure 6b); they changed due to the influence of the internal pollutant sources. This comparison was made with the one shown in Figure 4b. Moreover, it was observed that, for high *Ra* values, the temperature did not tend to homogenize as it did in the previous case, but a hot zone was formed at the top where the heat sources are located. This was because the convective flow led the heat transport from the heat sources to the upper part of the cavity. To describe the behavior of the mass transfer, the isoconcentrations formed by the internal pollutant sources were observed, as shown in Figure 6c. The isoconcentrations pattern was defined by the position of the pollutant sources. The behavior was similar to that shown in Figure 4c. Nevertheless, it could be seen that, due to the influence of the heat sources inside the cavity, the zone of influence of the concentration slightly grew around the pollutant sources.
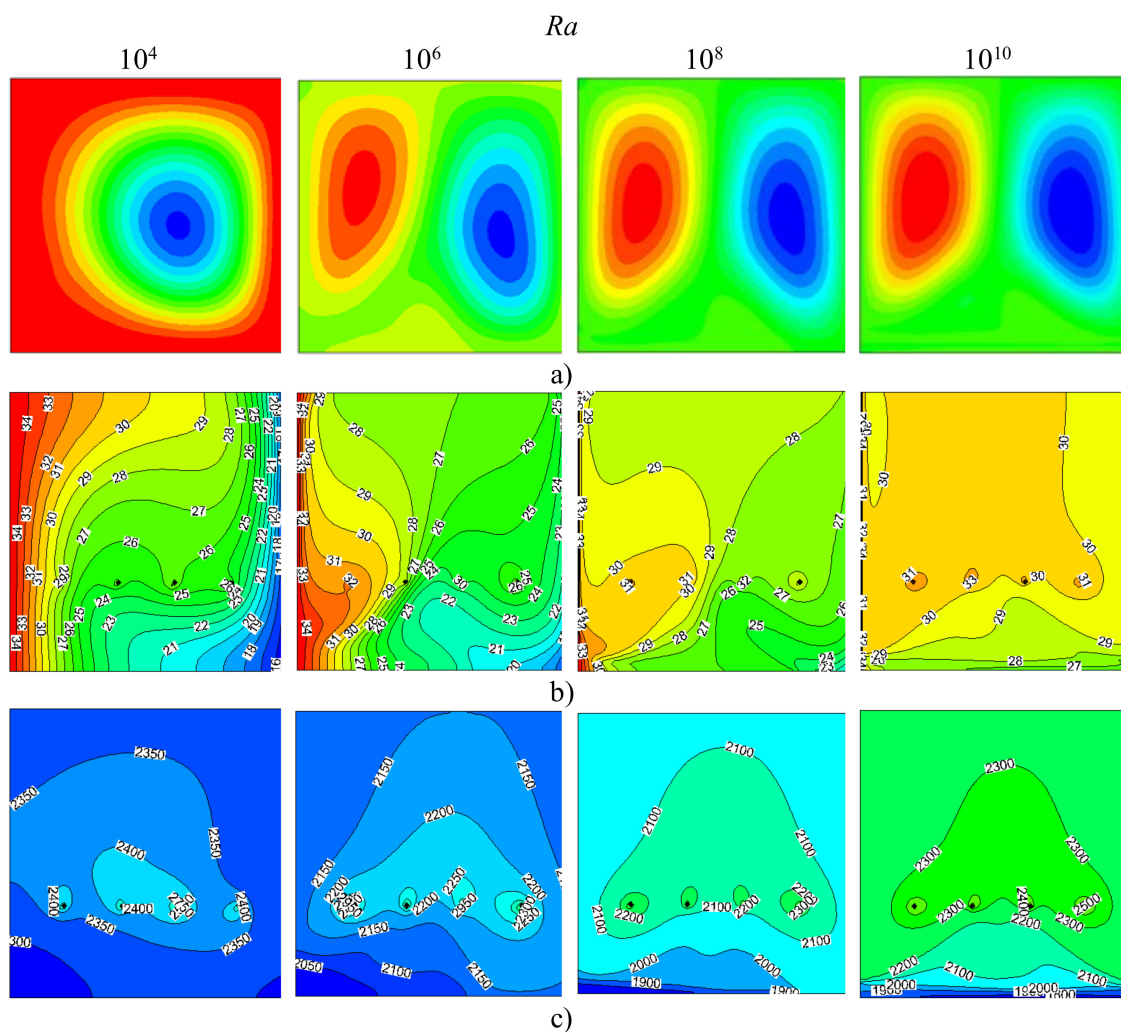

Figure 6. Effect of the heat and pollutant sources inside the cavity simultaneously: (**a**) flow patterns; (**b**) isotherms with internal heat sources; and (**c**) isoconcentrations with internal concentrations sources.

4.1. Analysis of the Temperatures and Concentrations at the Height of the Heat and Pollutant Sources

Hereafter, the graphs showing the temperature changes registered at the level of the heat sources are described. The temperature changes described occurred, in the first case, considering only heat sources and, in the second case, considering the double diffusion as a simultaneous effect when having both the heat and pollutant sources. Figure 7a shows that, when the pollutant sources were added, an increase and decrease in the temperatures was created around the areas close to the heat and

pollutants sources, respectively. Apart from that, when the Rayleigh number was increased to $Ra = 10^6$, according to Figure 7b, the temperatures remained high at the middle of the cavity, on the hot wall side. On the contrary, on the cold side, the temperatures were below the values in the scenario where only the differentially heated cavity was considered. The described behavior disappeared when the Ra value increased, in that from $Ra = 10^8$ the temperatures registered at the height of the heat sources increased by 5 °C approximately. This occurred in the first part of the cavity. For the value $Ra = 10^{10}$, the increase in the temperature was evident in the whole cavity. The results indicate the importance of the influence of the mass transfer on the heat transfer. Figure 7d shows that the behavior of the temperatures was analogous to with the heat sources alone but at a different intensity (5 °C, approximately).

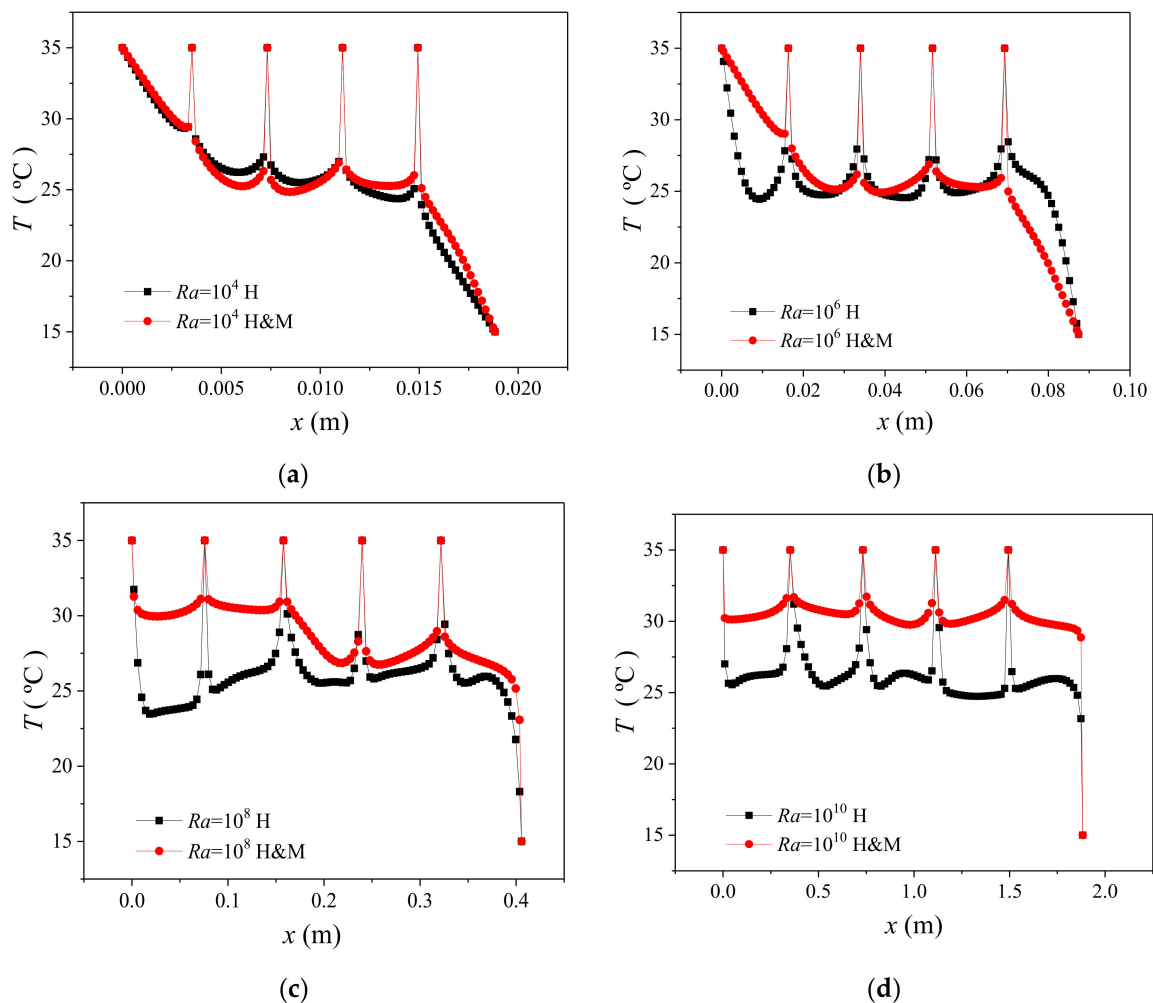**Figure 7.** Local temperatures at the height of the heat sources, for values of the Rayleigh number of (**a**) 10^4, (**b**) 10^6, (**c**) 10^8 and (**d**) 10^{10}. H (with heat sources) and HM (with heat and pollutant sources).

Figure 8 shows that the effect of the pollutant concentration sources, at the height where they are placed in the closed cavity, was similar to the other cases with the increase of the *Ra*. Furthermore, the values of pollutant concentration were not affected when the heat sources were added. This resulted in a low influence by the heat sources on the mass transfer. This almost non-existent influence was because the Dufourt effect was not considered. On the other hand, the effect of the mass transfer was defined by the rise of *Ra*; in this sense, there was a clear variation of approximately 100 ppm for the different values of *Ra* on the pollutant concentration levels.
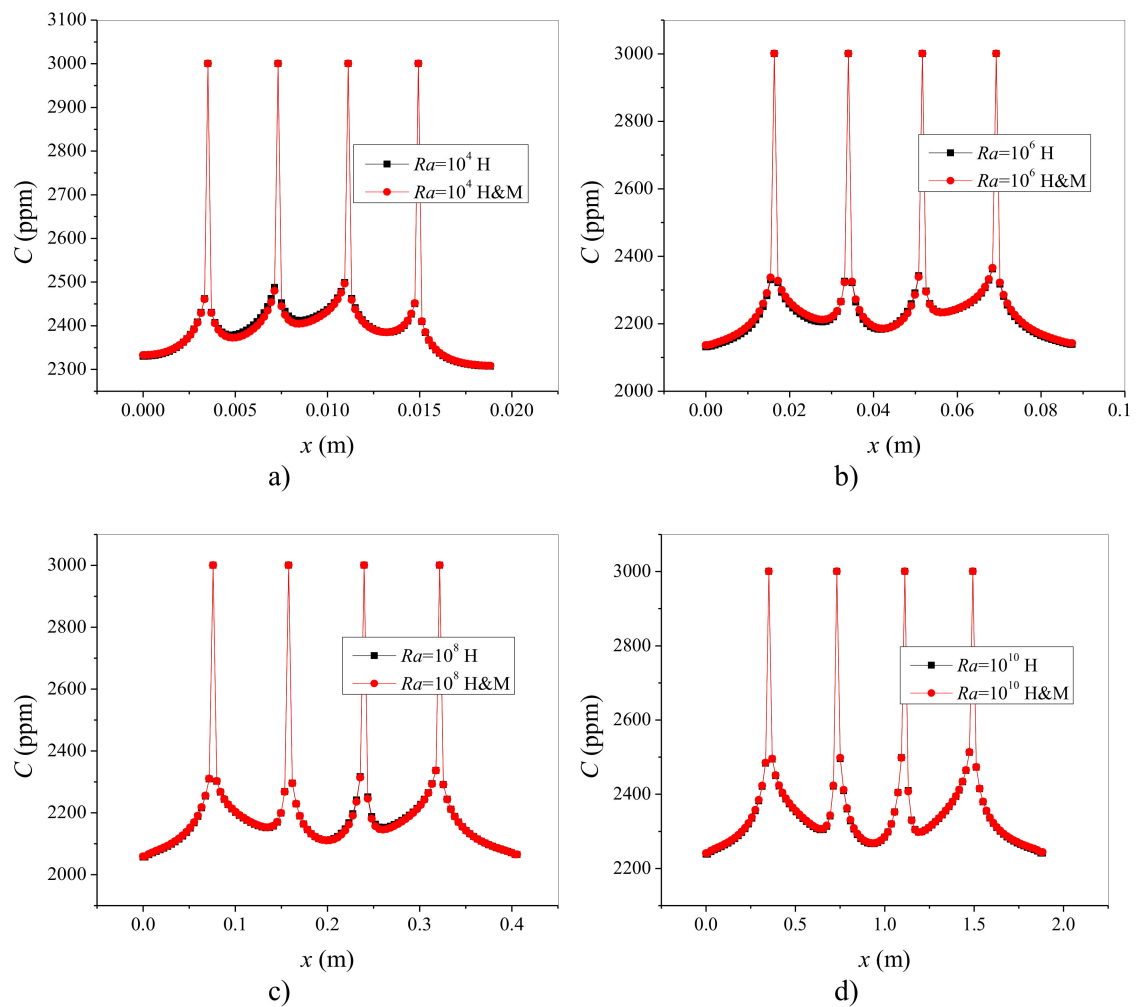
Figure 8. Local concentrations at the height of the simultaneous heat and pollutant sources, for values of the Rayleigh number of (**a**) 10^4, (**b**) 10^6, (**c**) 10^8 and (**d**) 10^{10}. H (with heat sources) and HM (with heat and pollutant sources).

In Table 2, the average values of temperature and pollutant concentration inside the closed cavity are shown. The values of the variables are presented for each value of the Rayleigh number. An increase in the temperature values, from 25.49 to 32.57 °C, was observed. On the contrary, for the pollutant concentration values, variations were obtained in the mean values; 2808 ppm was the highest value recorded. The registered values of the temperature and pollutant concentration variables changed due to the convective movement inside the cavity.

Table 2. Mean values inside the cavity.

Rayleigh Number			
10^4	10^6	10^8	101^0
Temperature (°C)			
25.49	26.34	27.99	32.57
Pollutant Concentration (ppm)			
2291	2808	2082	2781

4.2. Effect of the Pollutant Sources on the Heat Transfer

Figure 9 show the values of the local Nusselt number on the hot wall for the different values of the *Ra* number, in the case studies with heat sources and with heat and pollutant sources.

As shown in Figure 9, with the values $Ra = 10^4$, for the case of the configuration with internal heat sources, a behavior similar to that of the differentially heated cavity could be seen. However, the behavior changed for the same value of the *Ra* number with pollutant sources, due to the influence that they had inside the closed cavity. The pollutant sources showed a higher influence near the cold wall where the heat transfer diminished. In addition, when the value of the Rayleigh number at *Ra* = 10^6 increased, the behavior of the values of the local Nusselt number was nearly constant by the beginning of the hot wall and kept increasing up to near the top wall, where its value began to decrease again. For the value of the Rayleigh number at *Ra* = 10^8, the values of the Nusselt number took the shape of an inverted *C*, showing low values at the bottom and top parts of the vertical wall in the closed cavity, whereas in the central part of the wall the values of the Nusselt number tended to remain almost steady. Regarding the behavior of the Rayleigh number value $Ra = 10^{10}$, it was observed that the Nusselt number was practically steady along the hot wall, except near the bottom zone, where a sudden increase and decrease of the Nusselt number was recorded.
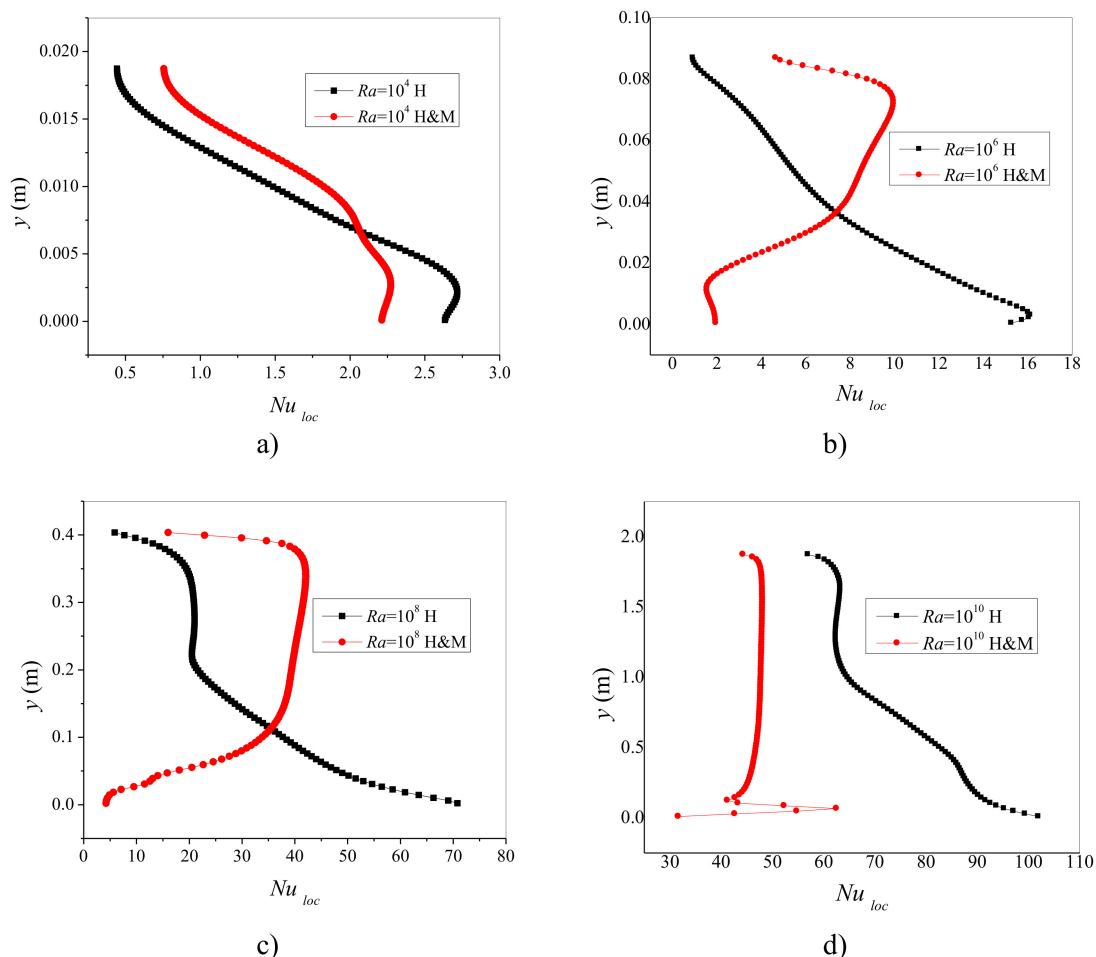

Figure 9. Local Nusselts numbers on the hot wall for values of the Rayleigh number of (**a**) 10^4, (**b**) 10^6, (**c**) 10^8, and (**d**) 10^{10}. H (with heat sources) and HM (with heat and pollutant sources).

4.3. Sherwood Number

In Figure 10, the values of the Sherwood number are shown for each value of the Rayleigh number in the present study. Figure 10 shows that the local values of the Sherwood number tended to decrease

in the middle zone of the hot and cold vertical walls. In contrast, for $Ra = 10^6$ (Figure 10b), it was observed that the local values of the *Sh* number were virtually zero for the left wall when there was only mass diffusion. However, when the double diffusion of heat and mass was performed, the convective flow had a change in direction, which in turn caused changes in the variable of the relative humidity concentration. On the right wall, it was observed that the values of the Nusselt number showed a similar behavior with the double diffusion of heat and mass. For the value $Ra = 10^8$, Figure 10c shows a change in the direction of the flow presented at the lower side on the right wall for the simple and double diffusion. By contrast, the values of the *Sh* number on the left and right walls were similar only when the double diffusion was performed. Finally, for the value of the Rayleigh number at $Ra = 10^{10}$, a change at the bottom on the right wall was registered, and the results were similar to the previous scenario when the double diffusion was performed.
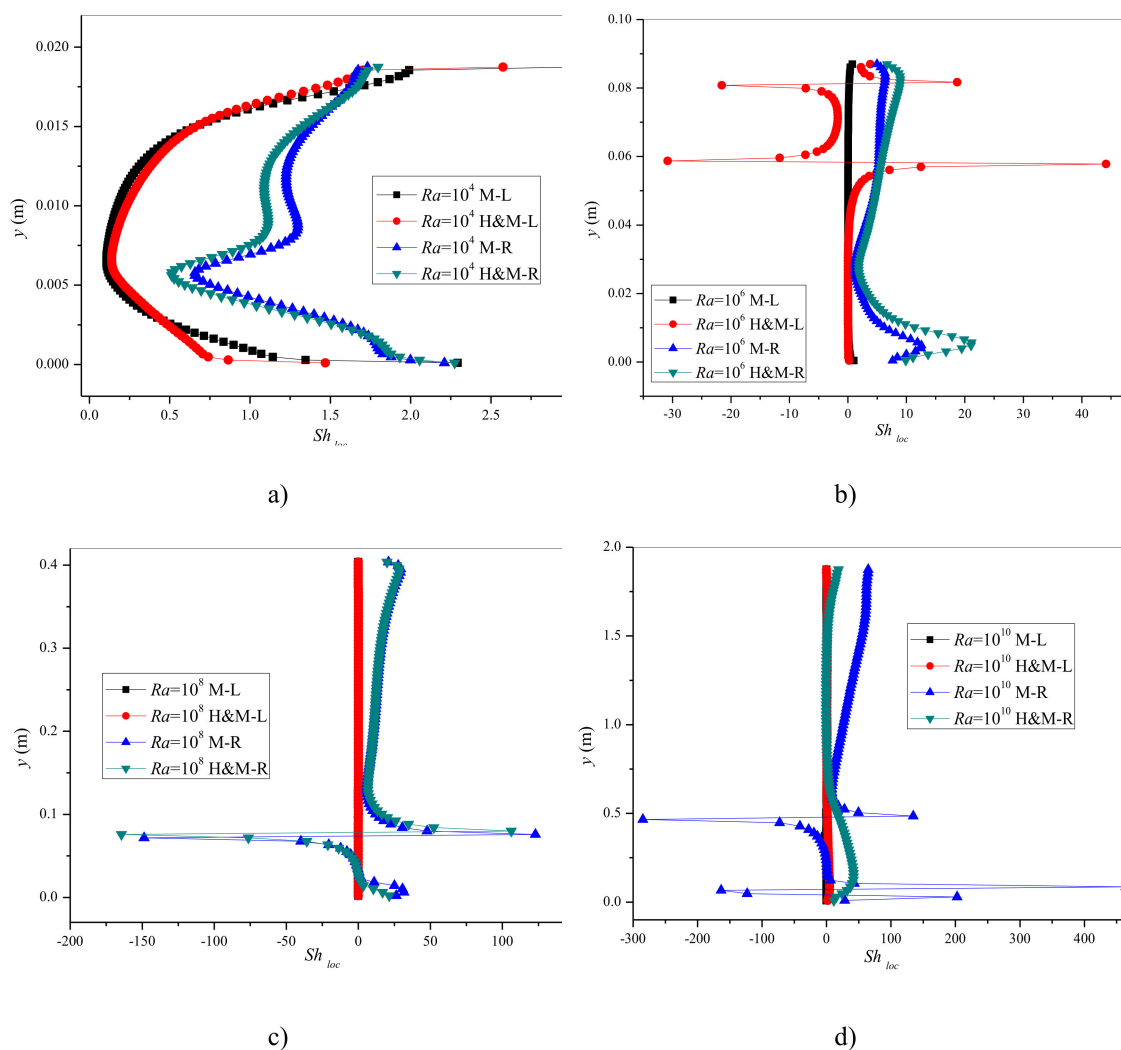

Figure 10. Local Sherwood numbers on the hot and cold wall for values of the Rayleigh number of (**a**) 10^4, (**b**) 10^6, (**c**) 10^8 and (**d**) 10^{10}. M (with pollutant sources), HM (with heat and pollutant sources), L (left wall), and R (right wall).

4.4. Average Values of the Nusselt and Sherwood Numbers

The average values of the Nusselt and Sherwood numbers on the vertical hot and cold walls are shown in Table 3. The values are presented for the simple diffusion case (A) and for the double diffusion case (B). The average values are presented for all the values of the Rayleigh number in this study. Table 3 shows that the values of the Nu number increased as the *Ra* number increased for either

simple diffusion or double diffusion. However, for the *Sh* number, the increase occurred during the simple diffusion for the hot wall; afterwards, there was a decrease in the *Sh* number in the double diffusion for $Ra = 10^8$ and $Ra = 10^{10}$, which was due to changes in the flow pattern inside the closed cavity, e.g., when there are flow direction changes. It was revealed that, for the cold wall, the values of the *Sh* number were very low and the behavior was very similar to that of the right wall.

Table 3. Average Nusselt and Sherwood numbers at the hot and cold walls.

Ra	Hot Wall		Cold Wall	
	Nu_{prom}	Sh_{prom}	Nu_{prom}	Sh_{prom}
10^4	1.60 [A]	1.32 [A]	2.73 [A]	0.005 [A]
	1.68 [B]	1.24 [B]	2.83 [B]	0.005 [B]
10^6	5.51 [A]	6.65 [A]	9.97 [A]	0.011 [A]
	7.31 [B]	4.79 [B]	9.98 [B]	0.006 [B]
10^8	15.99 [A]	12.36 [A]	35.66 [A]	0.025 [A]
	29.24 [B]	2.45 [B]	67.22 [B]	0.03 [B]
10^{10}	49.24 [A]	65.11 [A]	114.87 [A]	0.05 [A]
	52.69 [B]	10.82 [B]	126.35 [B]	0.06 [B]

A→Heat or Mass, B→Heat and Mass

5. Conclusions

A numerical study was carried out for an interval of the Rayleigh number from 10^4 to 10^{10}. Three case studies were analyzed: (1) closed cavity with heat sources; (2) closed cavity with pollutant sources; and (3) closed cavity with heat and pollutant sources. The results of the three case studies were compared. The heat and pollutant sources were placed (evenly distributed) at one third of the cavity's height, first separately and then simultaneously. It was found that, unlike the pollutant sources which dominated the flow pattern inside the cavity, the heat sources had little effect on the differentially heated cavity. It was found that the average values of temperature and concentration were 25.49 and 32.57 °C and 2082 and 2808 ppm, recorded as lower and higher values, respectively. It was found that the temperature increased as the Rayleigh number increased, but the pollutant concentration did not, because it increased or decreased when the Rayleigh numbers increased. The local values of the Nusselt number for the hot wall formed an X shape pattern for the case of the double diffusion with values of the Rayleigh number at $Ra = 10^6$ and $Ra = 10^8$. The average Nusselt number obtained its highest values in the simple diffusion case with the Rayleigh number at $Ra = 10^{10}$. The Sherwood numbers behaved similarly in the simple and double diffusion for low values of the Rayleigh number ($Ra = 10^4$); for the rest of the values of the Rayleigh number, the Sherwood numbers behaved similarly on the right vertical wall. It was found that placing heat and pollutant sources inside the cavity caused an increase or decrease of temperatures and pollutant concentrations, generating a flow pattern that is different to that of the differentially heated cavity. The flow recirculations had an effect on the values of temperature and pollutant concentration inside the cavity due to the heat and pollutant sources. Finally, other studies should be carried out to find the locations and intensities of the heat and pollutant sources that benefit the flow pattern to diminish the heat and pollutant concentrations inside the cavity.

Author Contributions: Conceptualization, J.S.-A.; methodology J.M.B.-F.; analysis of data, K.M.A.-C. and E.V.M.-M.; resources, J.X.; wrote the paper, J.S.-A.; All authors have read and approved the final manuscript.

Nomenclature

C	concentration of the pollutant or chemical species.
c_p	specific heat capacity.
D_{AB}	diffusion coefficient of the pollutant or chemical species.
D_t	coefficient of mass diffusion turbulent.
g_i	gravitational acceleration.
Hx	cavity width.
Hy	cavity height.
Nu	local Nusselt number.
n	normal direction.
p	fluid pressure.
P_{ref}	atmospheric pressure.
Pr	Prandtl number.
Ra	Rayleigh number.
$S\varphi$	source term.
S_{C_t}	turbulent Schmidt number.
T	temperature.
u	speed in the horizontal direction.
v	speed in the vertical direction.
x, y	coordinate x, y.
Greek	
α	thermal diffusivity.
β	coefficient of thermal expansion.
β_C	coefficient of volumetric expansion.
Γ	diffusion coefficient.
ε	dissipation of turbulent kinetic energy.
k	energy kinetic turbulent.
λ	thermal conductivity of the mixture.
μ	dynamic viscosity of the mixture.
μ_t	turbulent viscosity.
ν	kinematic viscosity of the mixture.
;	density of the mixture.
σ_t	turbulent Prandtl number.

References

1. Łukaszewicz, G.; Kalita, P. *Navier–Stokes Equations: An Introduction with Applications, Advances in Mechanics and Mathematics*; Springer International Publishing: Gewerbestrasse, Switzerland, 2016; Volume 34, pp. 1–387.
2. Das, D.; Basak, T. Role of distributed/discrete solar heaters during natural convection in the square and triangular cavities: CFD and heatline simulations. *Sol. Energy* **2016**, *135*, 130–153. [CrossRef]
3. Hua-Shu, D.; Gang, J. Numerical simulation of flow instability and heat transfer of natural convection in a differentially heated cavity. *Int. J. Heat Mass Transf.* **2016**, *103*, 370–381.
4. Mehedi, T.H.; Tahzeeb, R.B.; Islam, A.S. Numerical analysis of steady and transient natural convection in an enclosed cavity. *AIP Conf. Proc.* **2017**, *1851*, 020097.
5. Kouroudis, I.; Saliakellis, P.; Yiantsios, S.G. Direct numerical simulation of natural convection in a square cavity with uniform heat fluxes at the vertical sides: Flow structure and transition. *Int. J. Heat Mass Transf.* **2017**, *115*, 428–438. [CrossRef]
6. Kefayati, G.H.R. Simulation of natural convection and entropy generation of non-Newtonian nanofluid in a porous cavity using Buongiorno's mathematical model. *Int. J. Heat Mass Transf.* **2017**, *112*, 709–744. [CrossRef]
7. Miroshnichenko, I.V.; Sheremet, M.A. Radiation effect on conjugate turbulent natural convection in a cavity with a discrete heater. *Appl. Math. Comput.* **2018**, *321*, 358–371. [CrossRef]

8.   Parmananda, M.; Dalal, A.; Natarajan, G. The influence of partitions on predicting heat transfer due to the combined effects of convection and thermal radiation in cubical enclosures. *Int. J. Heat Mass Transf.* **2018**, *121*, 1179–1200. [CrossRef]

9.   Kefayati, G.H.R. Lattice Boltzmann method for natural convection of a Bingham fluid in a porous cavity. *Phys. A* **2019**, *521*, 146–172. [CrossRef]

10. Kamotani, Y.; Wang, L.W.; Ostrach, S.; Jiang, H.D. Experimental study of natural convection shallow enclosures with horizontal temperature and concentration gradient. *Int. J. Heat Mass Transf.* **1985**, *28*, 165–173. [CrossRef]

11. Benaccer, R.; Gobin, D. Coperating thermosolutal convection in enclosures-1. Scale analysis and mass transfer. *Int. J. Heat Mass Transf.* **1996**, *39*, 2671–2681. [CrossRef]

12. Gobin, D.; Benaccer, R. Coperating thermosolutal convection in enclosures-11. Heat transfer and flow structure. *Int. J. Heat Mass Transf.* **1996**, *39*, 2683–2697. [CrossRef]

13. Lee, J.; Hyun, L.W.; Kim, K.W. Natural convection in confined fluids with combined horizontal temperature and concentration gradients. *Int. J. Heat Mass Transf.* **1988**, *31*, 1969–1977. [CrossRef]

14. Van Der Eyden, J.T.; Van Der Meer, T.H.H.; Hanjalic, K. Double-diffusive natural convection in trapezoidal enclosures. *Int. J. Heat Mass Transf.* **1998**, *41*, 1885–1898. [CrossRef]

15. Joubert, P.; Le Quéré, P.; Béghein, C.; Collignan, B.; Couturier, S.; Glockner, S.; Groleau, D.; Lubin, P.; Musy, M.; Sergent, A.; et al. A numerical exercise for turbulent natural convection and pollutant diffusion in a two-dimensional partially partitioned cavity. *Int. J. Therm. Sci.* **2005**, *44*, 311–322. [CrossRef]

16. Zhao, F.Y.; Liu, D.; Tang, G.F. Natural convection in an enclosure with localized heating and salting from below. *Int. J. Heat Mass Transf.* **2008**, *51*, 2889–2904. [CrossRef]

17. Kuznetsov, G.V.; Sheremet, M.A. Conjugate heat transfer in an enclosure under the condition of internal mass transfer and in the presence of the local heat source. *Int. J. Heat Mass Transf.* **2009**, *52*, 1–8. [CrossRef]

18. Nikbakhti, R.; Rahimi, A.B. Double-diffusive natural convection in a rectangular cavity with partially thermally active side walls. *J. Taiwan Inst. Chem. Eng.* **2012**, *43*, 535–541. [CrossRef]

19. Chen, S.; Du, R. Entropy generation of turbulent double-diffusive natural convection in a rectangle cavity. *Energy* **2011**, *36*, 1721–1734. [CrossRef]

20. Ibrahim, A.; Lemonnier, D. Numerical study of coupled double-diffusive natural convection and radiation in a square cavity filled with A N_2-CO_2 mixture. *Int. Commun. Heat Mass Transf.* **2009**, *36*, 197–202. [CrossRef]

21. Serrano-Arellano, J.; Xamán, J.; Álvarez, G.; Gijón-Rivera, M. Heat and mass transfer by natural convection in a square cavity filled with a mixture of Air-CO_2. *Int. J. Heat Mass Transf.* **2013**, *64*, 725–734. [CrossRef]

22. Serrano-Arellano, J.; Gijón-Rivera, M.; Riesco-Ávila, J.M.; Elizalde-Blancas, F. Numerical study of the double diffusive convection phenomena in a closed cavity with internal CO_2 point. *Int. J. Heat Mass Transf.* **2014**, *71*, 664–674. [CrossRef]

23. Reid, R.C.; Prausnitz, J.M.; Poling, B.E. *The Properties of Gases and Liquids*; Mc Graw Hill: New York, NY, USA, 1987.

24. Jiménez-Xamán, C.; Xamán, J.; Gijón-Rivera, M.; Zavala-Guillén, I.; Noh-Pat, F.; Simá, E. Assessing the thermal performance of a rooftop solar chimney attached to a single room. *J. Build. Eng.* **2020**, *31*, 101380. [CrossRef]

25. El Mansouri, A.; Hasnaoui, M.; Amahmid, A.; Alouah, M. Numerical analysis of conjugate convection-conduction heat transfer in an air-filled cavity with a rhombus conducting block subjected to subdivision: Cooperating and opposing roles. *Int. J. Heat Mass Transf.* **2020**, *150*, 119375. [CrossRef]

26. Henkes, R.A.W.M. Natural Convection Boundary Layers. Ph.D. Thesis, Delft University of Technology, Delft, The Netherlands, 1990.

27. Olazo-Gómez, Y.; Xamán, J.; Gijón-Rivera, M.; Noh-Pat, F.; Simá, E.; Chávez, Y. Mathematical modelling of conjugate laminar and turbulent heat transfer in a cavity: Effect of a vertical glazed wall. *Int. J. Therm. Sci.* **2020**, *152*, 106310. [CrossRef]

28. Iyi, D.; Hasan, R. Numerical investigation of the effect of moisture on buoyancy-driven low turbulence flow in an enclosed cavity. *Int. J. Heat Mass Transf.* **2019**, *136*, 543–554. [CrossRef]

29. Patankar, S. *Numerical Heat Transfer and Fluid Flow*; Hemisphere Publishing: Washington, DC, USA, 1980.

30. Van Doormaal, J.; Raithby, G. Enhancements of the SIMPLE method for predicting incompressible fluid flow. *Numer. Heat Transf.* **1984**, *7*, 147–163. [CrossRef]

31. Béghein, C.; Haghighat, F.; Allard, F. Numerical study of double-diffusive natural convection in a square cavity. *Int. J. Heat Mass Transf.* **1992**, *45*, 833–846. [CrossRef]

32. Henkes, R.; Van-Der-Vlugt, F.; Hoogendoorn, C. Natural-convection flow in a square cavity calculated with low-Reynolds-number turbulence models. *Int. J. Heat Mass Transf.* **1991**, *34*, 377–388. [CrossRef]

33. Ampofo, F.; Karayiannis, T.G. Experimental Benchmark Data for Turbulent Natural Convection in Air Filled Square Cavity. *Int. J. Heat Mass Transf.* **2003**, *46*, 3551–3572. [CrossRef]